Cross-sectional Structural Analysis for 3D Printing Optimization

Nobuyuki Umetani[*] Ryan Schmidt[†]
Autodesk Research

Abstract

We propose a novel *cross-sectional structural analysis* technique that efficiently detects critical stress inside a 3D object. We slice the object into cross-sections and compute stress based on bending momentum equilibrium. Unlike traditional approaches based on finite element methods, our method does not require a volumetric mesh or solution of linear systems, enabling interactive analysis speed. Based on the stress analysis, the orientation of an object is optimized to increase mechanical strength when manufactured with 3D printing.

CR Categories: I.3.5 [Computer Graphics]: Computational Geometry and Object Modeling—Physically based modeling;

Keywords: structural analysis, optimization, 3D printing

1 Introduction

Democratized digital manufacturing devices such as desktop 3D printers enable non-professionals to casually create physical objects. Various software packages such as MeshMixer [Schmidt and Singh 2010] and Autodesk 123D [2010] provide end-users with intuitive 3D modeling interfaces for 3D printing. However, novice users often create structurally-unsound shapes which can easily break. Analyzing structural weakness is a significant challenge. Even simple rules-of-thumb may involve considering a large number of possible force location/magnitude combinations, and it is hard to estimate the effect of such forces on complex 3D shapes.

Umetani et al. [2012] showed that interactive analysis significantly helps novice users for plank-based furniture design. Our goal is to apply a similar concept for free-form 3D objects. Traditionally, structural validity of 3D objects was evaluated using the Finite Element Method (FEM). However, FEM involves time-consuming 3D mesh generation and the solution of large linear systems. As a result, FEM is generally not integrated into the real-time visualizations of interactive tools, making it difficult for users to consider structural robustness during incremental trial-and-error design.

To achieve fast shape validation, we propose *cross-sectional structural analysis*. We compute a number of cross sections of an object and compute forces on the cross sections. We extend the well-known Euler-Bernoulli assumption [Timoshenko 1970] to greatly reduce the complexity of the problem. The advantage of this assumption is that it focuses purely on the geometric relationship between a cross section and external load, ignoring deformation outside the cross section. Based on this simplification, we can find the weak parts of a 3D object at interactive rates.

[*]e-mail:n.umetani@gmail.com
[†]e-mail:ryan.schmidt@autodesk.com

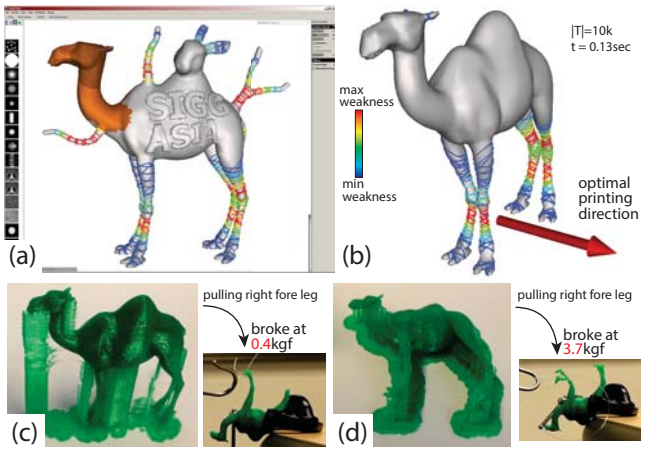

Figure 1: *(a) our system visualizes structural weakness at interactive rates during mesh editing. (b) A computed optimal printing direction. (c) A naïve printed model easily fractures under external force, while (d) the optimized print bears much larger forces.*

Our manufacturing target is 3D printing with the Fused Deposition Method (FDM). In this process, objects are constructed in layers, with each layer composed of a thin filament of melted plastic [Gibson et al. 2009]. This layer-by-layer construction introduces significant structural anisotropy – in particular, vertical bonding between layers is much weaker than the in-layer bonds. In this paper, we optimize the orientation of models for 3D printing to maximize their mechanical strength, based on our novel cross-sectional structural analysis.

2 Related Work

FEM has been applied for structural weakness detection to find the worst loading scenario [Zhou et al. 2013], to strengthen [Stava et al. 2012] and to partition [Luo et al. 2012] an input 3D object. We analyze structural weakness to optimize printing direction using novel cross-sectional structural analysis.

Make It Stand [Prévost et al. 2013] deforms objects so that they stand upright without toppling by optimizing momentum equilibrium under gravity. We similarly consider momentum equilibrium, but on cross sections under many different external forces.

Structural soundness has also been studied in graphics for masonry design (e.g. [Panozzo et al. 2013]). Whiting et al. [2012] propose a structural soundness evaluation function which considers bending force between bricks. In the same spirit, we consider bending force on cross sections to analyze structural soundness.

3 Method

Fracture criteria. Objects manufactured via layer-by-layer 3D printing techniques such as FDM exhibit significant anisotropy; they can bear considerable tensile force in the direction of filament strands, while being rather fragile when forces perpendicular to the filament strands are applied. Because FDM accumulates layers in a certain printing direction $\mathbf{\Theta} \in \mathbb{R}^3$, the printed object will frac-

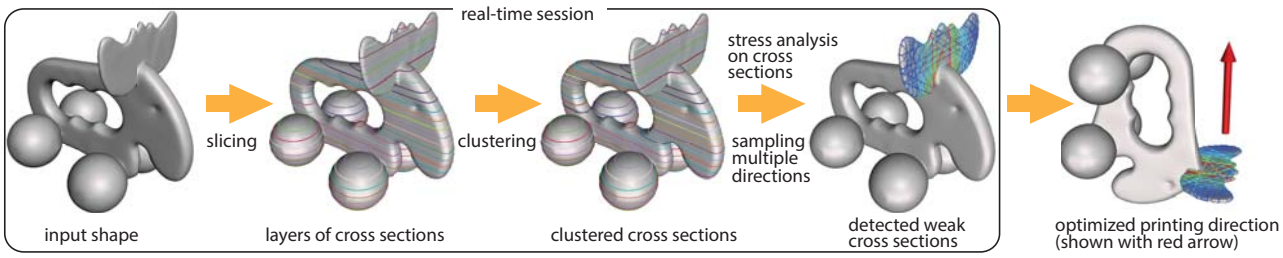

Figure 2: *Overview of our algorithm.*

ture much more easily in this direction. Within a layer, filament is usually oriented in many directions, so fracturing perpendicular to $\boldsymbol{\Theta}$ is significantly less likely. We denote $\hat{\sigma}_L$ as the maximum tensile stress under which a layer of filament separates. We conducted a simple experiment to break a cantilever beam and measured the value $\hat{\sigma}_L$ as 60MPa.

An overview of our algorithm is shown in Fig. 2. In detecting possible breaking scenarios, we first assume that an object is uniformly filled with an isotropic material which can bear maximum tensile stress $\hat{\sigma}_L$. Next, we find a set of cross sections for which external forces can produce a stress that exceeds $\hat{\sigma}_L$ inside that cross section. Then, we determine a printing direction $\boldsymbol{\Theta}$ such that the normal of the weakest cross sections are as perpendicular to $\boldsymbol{\Theta}$ as possible.

3.1 Cross-sectional Structural Analysis

Euler-Bernoulli assumption. Before describing our method, we briefly overview the Euler-Bernoulli (EB) assumption, on which our cross-sectional analysis is based. Assume a beam which has axis direction $\mathbf{z} \in \mathbb{R}^3$, a cross section Ω of the beam that is perpendicular to $\mathbf{z}$, and a line inside the beam – the *neutral axis* – which goes through the centroid of Ω (the neutral axis has direction $\mathbf{z}$). For a beams bending deformation, the assumption is threefold (see Fig. 3). First, there is no in-plane deformation and the cross section Ω remains planar. Second, the deformed Ω remains (approximately) perpendicular to the deformed neutral axis. Finally, the neutral axis does not stretch. Based on these assumptions, the infinitesimal strain tensor $\boldsymbol{\epsilon} \in \mathbb{R}^{3\times3}$ arising from bending is written as $\boldsymbol{\epsilon} = \epsilon \mathbf{z} \otimes \mathbf{z}$, where $\epsilon \in \mathbb{R}$ is a linear function over Ω and is zero at its centroid. This assumption is widely-used in the field of engineering. In the computer graphics literature, PriMo [Botsch et al. 2006] used a similar assumption of the rigidity of cross sections.

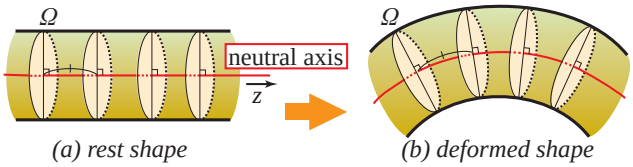

Figure 3: *Deformation of a beam under the Euler-Bernoulli assumption; The cross section Ω is rigid and remains perpendicular to the unstretched neutral axis.*

While the EB assumption is a widely-used engineering model, its application is traditionally limited to beam structures. Our challenge is to extend its application to free-form 3D objects. In this case, the assumption is reasonable if the representative length of a cross section Ω (e.g. circumradius) is much longer than the distance from Ω to the location the force is applied (i.e. moment arm). Hence, the assumption becomes more accurate as the cross-section thins and the moment-arm lengthens. Our key observation is that these are precisely the conditions in which fracture is most likely to occur, and hence we can still use this assumption for general 3D shapes for the purpose of critical stress detection.

Virtual cross-section. To implement the EB assumption on 3D objects, we first need to construct a cross section and neutral axis $(\Omega, \mathbf{z})$ such that $\mathbf{z}$ is perpendicular to Ω and passes through the centroid of Ω. Although the medial axis [Miklos et al. 2010] can be used to find candidates, the medial axis is costly to generate. Instead we introduce a fast *virtual cross section* technique to approximately generate $(\Omega, \mathbf{z})$. First, take an arbitrary cross section of the 3D object Γ which has a normal direction $\mathbf{n} \in \mathbb{R}^3$. We consider another section Γ' at a small distance Δn that has the same normal direction $\mathbf{n}$. For sections Γ and Γ', we compute the centroids $\mathbf{g}$ and $\mathbf{g}'$. Next, we compute a neutral axis direction Γ as $\mathbf{z} = (\mathbf{g}' - \mathbf{g})/|\mathbf{g}' - \mathbf{g}|$ with infinitesimally-small distance $\Delta n \to 0$. Finally, we get a virtual cross-section Ω by projecting Γ perpendicular to $\mathbf{z}$ so that the centroid of Ω remains $\mathbf{g}$.

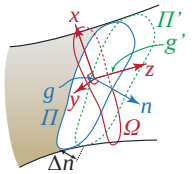

We consider the local coordinate $\mathbf{x}$ and $\mathbf{y}$ on the virtual cross section Ω taking the origin at centroid $\mathbf{g}$. We define axis $\mathbf{y}$ such that it is on the original section Γ. If the angle between $\mathbf{n}$ and $\mathbf{x}$ – denoted θ – is large, the virtual section is no longer a good approximation of an actual section in the direction of $\mathbf{z}$. Hence, we discard sections where $\theta > 45°$. We consider a fixed set of sample directions for $\mathbf{n}$, specifically the 13 unique directions of the form $(A, B, C)^T$, where each of A, B, C takes the values $(-1, 0, +1)$.

External bending moment. Given a virtual cross section and its neutral axis direction $(\Gamma, \mathbf{n}) \to (\Omega, \mathbf{z})$, we now consider bending moment equilibrium to compute the stress on Ω. We assume the external force $\mathbf{f}$ is applied at a point $\mathbf{p}$ on the object's surface. The resulting external bending moment $\boldsymbol{\tau}^{ex} \in \mathbb{R}^3$ which rotates the virtual cross section can be written as

$$\boldsymbol{\tau}^{ex} = (\mathbf{I} - \mathbf{z} \otimes \mathbf{z}) \{(\mathbf{p} - \mathbf{g}) \times \mathbf{f}\}, \tag{1}$$

where $\mathbf{I}$ is an identity matrix. Note that $\boldsymbol{\tau}^{ex}$ is in the plane of Ω. To achieve momentum equilibrium, the virtual cross section must generate a bending moment which balances out this external moment.

Internal bending moment. Using the EB assumption, we can denote $\mathbf{z}$-directional strain as a linear function of $\mathbf{xy}$-coordinate $\epsilon(x, y) = \bar{\epsilon}_X x + \bar{\epsilon}_Y y$. From Hooke's law, $\mathbf{z}$-directional stress is given as $\sigma = E\epsilon$ where E is the Young's modulus. We define orthogonal axes $\boldsymbol{\xi}$ and $\boldsymbol{\eta}$ such that strain is zero $(\bar{\epsilon}_X x + \bar{\epsilon}_Y y = 0)$ on the axis $\boldsymbol{\xi}$. Let ψ be the angle between $\boldsymbol{\xi}$ and $\mathbf{x}$. With this axis transformation, the strain can be denoted in $\boldsymbol{\xi\eta}$-coordinate as $\epsilon(\xi, \eta) = \bar{\epsilon}_\xi \eta$, where $\bar{\epsilon}_\xi = \bar{\epsilon}_X \cos\psi + \bar{\epsilon}_Y \sin\psi$. The Internal

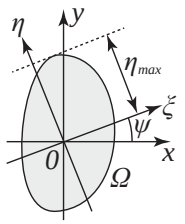

bending moment vector then becomes:

$$\boldsymbol{\tau}^{in} = \int_{\Omega} \eta(E\epsilon)d\Omega\boldsymbol{\xi} = \bar{\epsilon}_{\xi} E I_{\xi} \boldsymbol{\xi}, \tag{2}$$

where I_ξ is the *second moment of area*: $I_\xi = \int_\Omega \eta^2 d\Omega$.

Moment equilibrium. Considering the moment equilibrium $\boldsymbol{\tau}^{ex} + \boldsymbol{\tau}^{in} = 0$, we obtain $\boldsymbol{\xi} = \boldsymbol{\tau}^{ex}/|\boldsymbol{\tau}^{ex}|$ and $\bar{\epsilon}_\eta = |\boldsymbol{\tau}^{ex}|/(EI_\xi)$. The maximum stress on the virtual cross section can be written as $\sigma_{max} = |\boldsymbol{\tau}^{ex}|/Z_\xi$, where $Z_\xi = I_\xi/|\eta|_{max}$ and $|\eta|_{max}$ is the maximum of the absolute value of coordinate η inside this virtual cross section. In the engineering literature, Z_ξ is called the *section modulus*, relating the bending moment and maximum stress. When σ_{max} exceeds $\hat{\sigma}_L$, this section may fracture. Note that the maximum stress does not depend on the Young's modulus or other material parameters; based on the cross-section's shape, force position, and its direction, we can estimate stress inside the object in a purely geometric manner.

Clustering cross-sections. So far, we have described a way to compute maximum stress on a cross section, given an external force. However, in a complex shape, there may be multiple disjoint cross-sections in a single slice, and the distribution of forces depends on the boundary conditions (i.e. where the object is fixed, and where the external force is applied). Hence, for a group of planar cross sections, we divide the object into two connected surfaces S^+ and S^-, with S^+ having smaller area than S^-. Then, we apply the force somewhere on S^+ and fix the object at a point somewhere on S^-. The motivation for this heuristic is that we usually hold the larger part of an object when applying a force. Fig. 4 illustrates this process. First, we compute all cross-sections of an object $\{\gamma_1, \gamma_2, \ldots\}$ in a given plane. Then, we greedily cluster these sections into groups $\boldsymbol{\Gamma} := \{\Gamma_1, \Gamma_2, \ldots\}$ such that each group's sections $\Gamma_i \in \boldsymbol{\Gamma}$ divide the object into a S^+ and S^-. Each group is formed by picking an initial section γ_i, and then for remaining sections γ_j, checking if a path from γ_i to γ_j exists on each side of the section plane. If so, γ_j is clustered with γ_i. We iterate this process until all the sections have been separated into groups, and then for each group Γ_i, we compute the virtual cross section Ω_i.

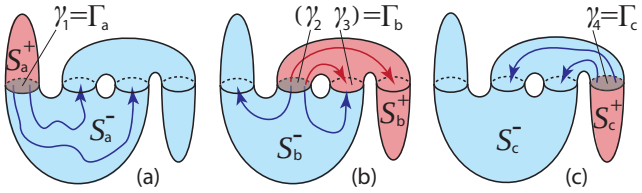

Figure 4: *Three alternatives for separation of an example object into surfaces S^+ (red) and S^- (blue). We apply force at somewhere on S^+. The cross-sections are grouped as $\{\Gamma_a, \Gamma_b, \Gamma_c\} = \{\gamma_1, (\gamma_2, \gamma_3), \gamma_4\}$. As shown in (b), γ_2 and γ_3 are in the same group because it is connected from both side.*

Clustering Computation. To efficiently determine if sections are connected, we use a connectivity graph. We first compute sections of the object at interval h along $\mathbf{n}$ (we use $h = 32$). Next we construct a section adjacency graph, where sections are connected if there is a path of triangles between them that does not cross other sections (Fig. 5-left). We can then quickly determine if sections are accessible from both sides using this adjacency information (Fig. 5-right). Finally, for each section Γ_i we denote the set of other sections that lie on S_i^+ as $\boldsymbol{\Gamma}_i^+$, which will be used for approximate integration in the next section.

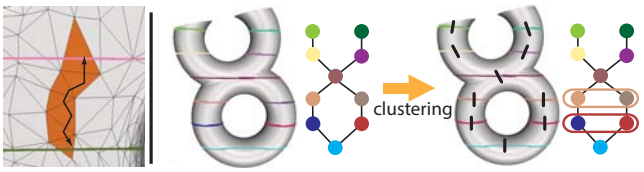

Figure 5: Left: *two cross sections are adjacent if triangles are connecting them without crossing other sections.* **Right:** *sections in the same plane are grouped based on adjacency information. The neutral axis (black line) is computed for each section group.*

3.2 Optimized 3D Printing Direction

The result of the analysis technique described above is a large number of combinations of cross section and external force. Next we must detect which section/force pairs are most likely to break.

Weakness evaluation. Structural weakness of a cross section is defined considering two factors; the magnitude of force needed to break a section, and the area over which the force is distributed. Let $\mathbf{f}_{min}(\Gamma, \mathbf{p}, \psi)$ be the minimal force at position $\mathbf{p}$ on the surface needed to produce the critical stress on section Ω with bending direction ψ. From Eq.(1) and Eq.(2), we have

$$\mathbf{f}_{min}(\Gamma, \mathbf{p}, \psi) = |(\mathbf{I} - \boldsymbol{\xi} \otimes \boldsymbol{\xi})(\mathbf{p} - \mathbf{g})|\, \hat{\sigma}_L Z_\xi \boldsymbol{\eta} \tag{3}$$

Next we define a function $B(\Gamma, \mathbf{p}, \psi)$ which indicates the relative ease with which a section/force configuration can be broken. B is defined as $1/\mathbf{f}_{min}$ if $|\mathbf{f}_{min}| < \hat{f}_{max}$, and 0 otherwise, where $\hat{f}_{max}$ is a maximum external force (we choose 0.2 kgf). We then define the relative *weakness* of a section Γ_i by integrating B over the potential force point locations on S^+

$$W(\Gamma_i) = \int_{s \in S_i^+} \int_{2\pi} B(\Gamma_i, \mathbf{p}(s), \psi) d\psi ds, \tag{4}$$

where $\mathbf{p}(s)$ is the position of force point at a surface point s. We approximate this costly surface integral by computing only on the sections. Since the input shape is a triangle mesh, its cross sections are polylines. Thus, we compute the integration by aggregating B multiplied by l_m, which is half the sum of the two neighboring edge lengths for the vertex s_m on a polyline. Furthermore, ψ is sampled at intervals J (we used $J = 16$):

$$W(\Gamma_i) \simeq \frac{2\pi h}{J} \sum_{\Gamma_k \in \boldsymbol{\Gamma}_i^+} \sum_{s_m \in \Gamma_k} l_m \sum_{j=1}^{J} B\left(\Gamma_i, \mathbf{p}(s_m), \frac{2\pi j}{J}\right), \tag{5}$$

We further accelerate computation by culling sections $\Gamma_k \in \boldsymbol{\Gamma}_i^+$ which cannot break the cross section Γ_i. This is accomplished by computing the bounding volume of Γ_k (we used the circumcircle as a bounding volume) and checking that the minimum breaking force $|\mathbf{f}_{min}|$ is larger than the maximum-force threshold $\hat{f}_{max}$ for all points on the section.

Print Orientation Optimization. Using the machinery described thus far, we can proceed to optimize the object orientation for printing. For a set of given normal directions $\mathbf{n}$, we slice the object at intervals h and compute our weakness metric $W(\Gamma_i)$ for all sections, and then store the identified "weak" sections as $\boldsymbol{\Gamma}^w := \{\Gamma_j \in \boldsymbol{\Gamma}^w | W(\Gamma_j) \neq 0\}$. Once the weak cross-sections are detected, we need only to select an optimal printing direction. As we previously mentioned, objects printed with FDM are mostly

likely to break between layers. Since the bending moment excites force in the direction of neutral axis $\mathbf{z}$, the object should be oriented such that $\mathbf{z}$ is as vertical as possible. Hence, we use our weakness metric to weight the neutral axis directions $\mathbf{z}_j$ corresponding to identified weak sections Γ_j, and then obtain the optimal printing direction $\mathbf{\Theta}_{opt}$ as

$$\mathbf{\Theta}_{opt} = \underset{\mathbf{\Theta}\in\mathbb{R}^3, |\mathbf{\Theta}|=1}{\arg\min} \sum_{\Gamma_j \in \mathbf{\Gamma}^w} \mathbf{\Theta} \cdot W(\Gamma_j)\mathbf{z}_j. \quad (6)$$

Eq. (6) can be solved by eigen-analysis of a 3x3 symmetric positive definite matrix $\sum_{\Gamma_j \in \mathbf{\Gamma}^w} W(\Gamma_j)\mathbf{z}_j \otimes \mathbf{z}_j$. The smallest eigenvector gives the strongest printing direction $\mathbf{\Theta}_{opt}$. Note that in some cases no printing direction can strengthen all weak cross sections. However we have observed that such cases are rare.

4 Results

In Fig. 6, we compare our method with a standard second-order linear FEM stress analysis. The force distribution on two different virtual cross sections is displayed. As expected, when the initial section is relatively orthogonal to the local surface, so is the virtual section, and the force magnitude/directions agree well with the ground-truth FEM. As the virtual section diverges from the original section, the directions necessarily diverge as well, but the maximum magnitudes remain comparable. Unlike FEM, our method is not affected by the quality of the surface mesh. Degenerate and "skinny" sliver triangles are common in CAD meshes, but they do not affect our computation (see Fig. 7-rightmost).

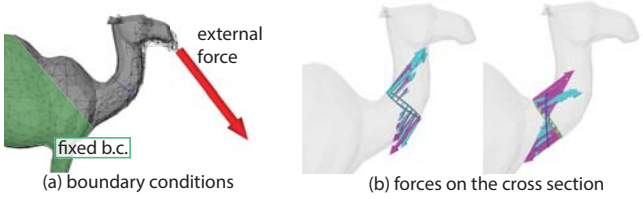

Figure 6: *Comparison with FEM. Cyan vectors show FEM forces, purples are ours, blue loops are original input cross section, and green loops are virtual cross sections.*

We also implemented our technique in a 3D mesh modeling tool [Schmidt and Singh 2010]. The accompanying video shows interactive modeling sessions with our structural analysis running on a background thread, and updating real-time visualizations when the model is edited. Fig. 7 shows weak regions, optimal printing directions, and computation times for various objects. Our algorithm scales well up to detailed meshes. In the video, we see the visualization update for a mesh with 650k triangles in a few seconds.

We 3D printed several models shown in the figures, and applied forces to evaluate their strength (see Fig. 1 and accompanying video). We used the MakerBot Replicator 2 and MakerWare v2.2 for printing, with the objects printed as solid (100% infill) to maximize strength. The material we used was polylactic acid (PLA) filament. Our algorithm assumes the object breaks with bending force, hence it cannot handle complex fracture such as buckling. However, we observed that the locations where objects fracture agreed well with the weakest cross-sections our algorithms identified, and that our optimal orientation makes objects significantly stronger.

5 Conclusion

We present a framework for structural weakness detection of 3D objects which is fast enough to provide real-time feedback during 3D shape editing. Based on this analysis we optimize the orientation of the model for 3D printing to increase structural soundness.

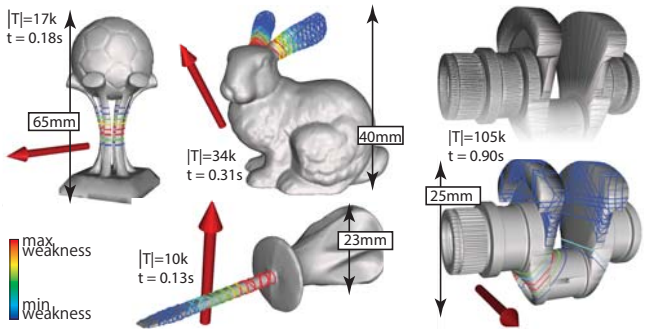

Figure 7: *More examples. $|T|$ is the triangle count, and t is the total time taken to compute our cross-sectional analysis (using an Intel Xeon™ 2.5 GHz CPU machine). Red arrows show the optimal printing directions.*

References

AUTODESK, 2010. Autodesk 123d. http://www.123dapp.com/.

BOTSCH, M., PAULY, M., GROSS, M., AND KOBBELT, L. 2006. PriMo: coupled prisms for intuitive surface modeling. In Proc. of the 4th Eurographics Symp. on Geom. Proc., SGP '06, 11–20.

GIBSON, I., ROSEN, D. W., AND STUCKER, B. 2009. Additive Manufacturing Technologies: Rapid Prototyping to Direct Digital Manufacturing, 1st ed. Springer Publishing, Inc.

LUO, L., BARAN, I., RUSINKIEWICZ, S., AND MATUSIK, W. 2012. Chopper: partitioning models into 3D-printable parts. ACM Trans. Graph. 31, 6 (Nov.), 129:1–129:9.

MIKLOS, B., GIESEN, J., AND PAULY, M. 2010. Discrete scale axis representations for 3D geometry. ACM Trans. Graph. 29 (July), 101:1–101:10.

PANOZZO, D., BLOCK, P., AND SORKINE-HORNUNG, O. 2013. Designing unreinforced masonry models. ACM Trans. Graph. 32, 4 (July), 91:1–91:12.

PRÉVOST, R., WHITING, E., LEFEBVRE, S., AND SORKINE-HORNUNG, O. 2013. Make it stand: balancing shapes for 3d fabrication. ACM Trans. Graph. 32, 4 (July), 81:1–81:10.

SCHMIDT, R., AND SINGH, K. 2010. MeshMixer: an interface for rapid mesh composition. ACM SIGGRAPH 2010 Talks.

STAVA, O., VANEK, J., BENES, B., CARR, N., AND MĚCH, R. 2012. Stress relief: improving structural strength of 3D printable objects. ACM Trans. Graph. 31, 4 (July), 48:1–48:11.

TIMOSHENKO, S. 1970. Theory of Elasticity, 3 ed. Mcgraw-Hill College, 6.

UMETANI, N., IGARASHI, T., AND MITRA, N. J. 2012. Guided exploration of physically valid shapes for furniture design. ACM Trans. Graph. 31, 4 (July), 86:1–86:11.

WHITING, E., SHIN, H., WANG, R., OCHSENDORF, J., AND DURAND, F. 2012. Structural optimization of 3D masonry buildings. ACM Trans. Graph. 31, 6 (Nov.), 159:1–159:11.

ZHOU, Q., PANETTA, J., AND ZORIN, D. 2013. Worst-case structural analysis. ACM Trans. Graph. 32, 4 (July), 137:1–137:12.